Supramolecular Nanoarchitectures

DOI: 10.1002/anie.201004127

Controlling the Transformation of Primary into Quaternary Structures: Towards Hierarchically Built-Up Twisted Fibers**

Juan Luis López, Carmen Atienza, Wolfgang Seitz, Dirk M. Guldi, and Nazario Martín**

Dedicated to Professor Antonio García Martinez on the occasion of his 70th birthday

The construction of self-assembling and replicating structures that bear photonic and/or electronic active units at the nanometric scale constitutes one of the biggest challenges in contemporary science.[1] In the bottom-up approach, control over the self-organizing constituents of unprecedented one-, two-, and three-dimensional nanostructured materials at different length scales is of primary interest for the fine-tuning of electronic and optical properties. Leading examples of truly sophisticated architectures contain photo- and redoxactive constituents, such as porphyrins,[2] hexabenzacoronenes,[3] oligo(*p*-phenylene)vinylenes,[4] tetrathiafulvalene,[5] perylene bisimides,[6] and fullerenes,[7] all of which—with the exception of the spherical fullerenes—have planarity in common as a templating motif. Notably, concave curved polycyclic aromatic hydrocarbons (PAHs; e.g., corannulenes) support supramolecular ensembles that are based on face-to-face interactions between complementary π surfaces; however, only a few examples have been reported to date.[8]

Our research group has pioneered the use of 2-[9-(1,3-dithiol-2-ylidene)anthracen-10(9*H*)-ylidene]-1,3-dithiole (π-extended tetrathiafulvalene, π-exTTF) derivatives, which have concave curved anthracene cores, as topographic templates for fullerenes.[9] In these system, fullerene recognition, which is thermodynamically driven by concave–convex complementarity combined with electronic interactions and charge transfer, induces the self-association of the constituents into a variety of supramolecular ensembles, such as oligomers/polymers and dendrimers. However, to the best of our knowledge, the 3D ordering of *p*-quinoid π-exTTF units into nanometric arrays in solution is unprecedented. Inspired by the manifold possibilities of "curved" scaffolding π-exTTF species, we have now explored the creation of novel photo- and electroactive 3D nanoarchitectures. We focused on the use of **1**, a well-known and versatile hydrogen-bonding building block,[10,11] and **2**, which consists of a hydrogen-bonding diamino-*s*-triazine, a π-conjugated *p*-phenylenevinylene spacer, and π-exTTF (Figure 1). Brought together, for example in solution, **1** and **2** self-assemble into **1·2**.

Compound **2** was synthesized from 2-(*p*-cyanophenyl)-vinyl-π-exTTF and dicyanamide and characterized by standard spectroscopic techniques (see the Supporting Information). Compound **1** was prepared in accordance with previously reported experimental procedures.[12]

^{1}H NMR spectroscopic studies in $CDCl_3$ confirmed the hydrogen-bonding interactions of the constituents to afford complex **1·2**, for which 1:1 or 2:1 stoichiometries are possible. In particular, in the ^{1}H NMR spectrum of **1** (8×10^{-4} M), the N–H proton resonances were observed as a singlet at $\delta = 7.75$ ppm, whereas the NH_2 proton resonances of **2** (8×10^{-4} M) appeared as a single, broad signal at $\delta = 5.14$ ppm. Throughout the titration assays, a significant downfield shift was discernable for the imide hydrogen atoms of **1** (8×10^{-4} M), from $\delta = 7.75$ to 7.96 ppm. This downfield shift implies that, at room temperature, the N–H imide hydrogen atoms form hydrogen bonds in $CDCl_3$ with **2** (see Figure S1 in the Supporting Information).[13] In contrast, no appreciable shifts were observed for assays in either CD_3CN or [D_8]THF in similar concentration ranges (see Figure S2 in the Supporting Information).

Hydrogen-bonding interactions in **1·2** were also deduced from FTIR spectra in methylcyclohexane (MCH) and $CHCl_3$ (see Figure S4 in the Supporting Information). In the absence of **2**, the imide carbonyl stretching bands of **1** appeared at around 1774–1685 cm^{-1}, whereas in **1·2** the stretching was observed at frequencies of 1724, 1607, 1458, and 1406 cm^{-1}. Likewise, the N–H stretching of **2** at 3199 and 3340 cm^{-1} was invisible in an equimolar mixture of **1** and **2** in both MCH and $CHCl_3$. Corresponding experiments in CH_3CN are best described as the simple superimposition of the individual IR spectra and thus indicated noninteracting constituents (see Figure S5 in the Supporting Information).

[*] Dr. J. L. López, Dr. C. Atienza, Prof. N. Martín
Departamento de Química Orgánica, Facultad de C. C. Químicas
Universidad Complutense de Madrid, 28040 Madrid (Spain)
Fax: (+34) 91-394-4332
and
IMDEA-nanociencia
28049 Madrid (Spain)
Fax: (+34) 91-394-4103
Dr. W. Seitz, Prof. D. M. Guldi
Department Chemie und Pharmazie and
Interdisciplinary Center for Molecular Materials
Universität Erlangen-Nürnberg
Egerlandstrasse 3, 91058 Erlangen (Germany)
Fax: (+49) 9131-85-28307
E-mail: nazmar@quim.ucm.es
guldi@chemie.uni-erlangen.de
Homepage: http://www.ucm.es/info/fullerene

[**] Financial support by the Ministerio de Ciencia e Innovación (MICINN) of Spain (projects CTQ2008-00795/BQU and Consolider-Ingenio CSD2007-00010), the EU (FUNMOLS FP7-212942-1), and the CAM (MADRISOLAR-2 project S2009/PPQ-1533) is acknowledged. We also thank the Deutsche Forschungsgemeinschaft (SFB583) and the Office of Basic Energy Sciences of the US. We thank Prof. E. Ortí (ICMol) for the preliminary theoretical calculations. J.L.L. thanks the Fundación Séneca, CARM of Spain, for a postdoctoral fellowship.

Supporting information for this article is available on the WWW under http://dx.doi.org/10.1002/anie.201004127.

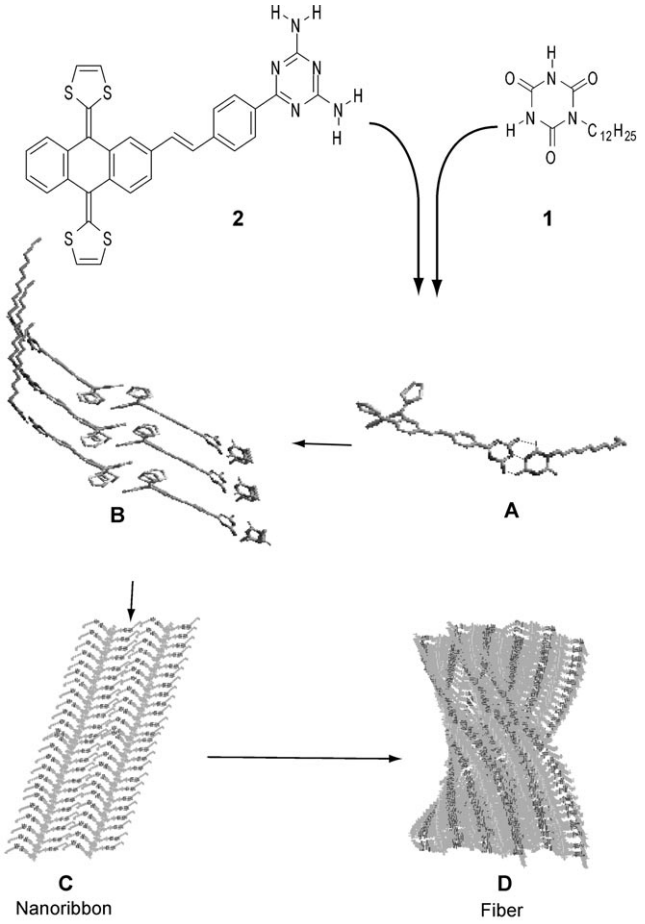

Figure 1. Primary, secondary, tertiary, and quaternary supramolecular structures **A**–**D** proposed to form from compounds **1** and **2**.

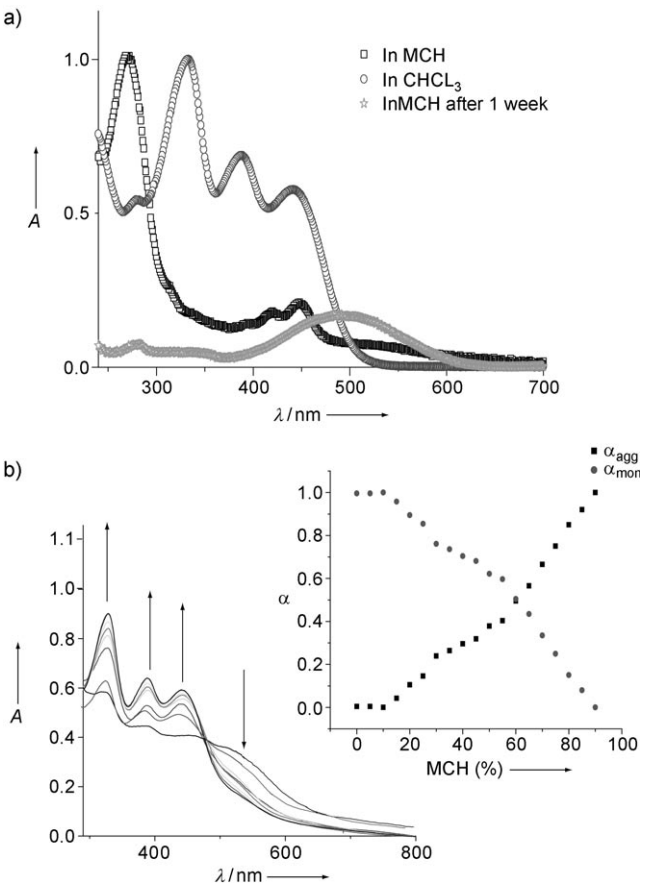

Figure 2. a) UV spectra of a 1:1 mixture of **1** and **2** in $CHCl_3$ (open circles) and in methylcyclohexane (open squares), and of the bright-orange solid obtained after aging of the mixture in MCH (open stars). b) Solvent-dependent UV/Vis absorption spectra of the partially diluted aged solution (1.25×10^{-4} M) in various MCH/$CHCl_3$ mixtures. Arrows indicate the spectral changes upon increasing the amount of $CHCl_3$ (from 0 to 100%). A plot of α_{agg} (solid squares) and the mole fraction of the monomer (α_{mon}, solid circles) versus the amount of MCH is shown in the inset.

Additional insight into the interaction of **1** and **2** was obtained from absorption assays in MCH and $CHCl_3$. For **2** in $CHCl_3$, absorption maxima were observed at 331 ($\varepsilon = 29759\,M^{-1}cm^{-1}$), 387 ($\varepsilon = 20454\,M^{-1}cm^{-1}$), and 441 nm ($\varepsilon = 19870\,M^{-1}cm^{-1}$). Upon the incremental addition of **1** to a solution of **2** (2.5×10^{-4} M) in $CHCl_3$, the only notable change was an overall increase in absorption; no appreciable shifts were observed (see Figure S6a in the Supporting Information). In MCH, a significantly different spectrum with lower extinction coefficients was observed, with bands at 392 ($\varepsilon = 850\,M^{-1}cm^{-1}$), 419 ($\varepsilon = 1000\,M^{-1}cm^{-1}$), and 447 nm ($\varepsilon = 5880\,M^{-1}cm^{-1}$) followed by a shoulder at 500 nm ($\varepsilon = 404\,M^{-1}cm^{-1}$; see Figure S6b in the Supporting Information). Again, no significant changes were observed in the presence of **1**. The broad and structureless bands observed in the UV/Vis spectra of **2** when apolar MCH was used as the solvent instead of polar chloroform (see Figure S6 in the Supporting Information) strongly suggest that aggregation occurs in MCH, with the onset ranging up to 700 nm.

A completely different scenario evolved when **1·2** was left to age in, for example, MCH. Now, the absorption spectra were characterized by intensification of the shoulder at 500 nm and concomitantly decreasing features in the 300–450 nm range (Figure 2a). In control experiments with **2** alone (2.5×10^{-4} M), no differences were detected during aging (see Figure S7 in the Supporting Information). The overall bathocromic shift of around 50 nm attests π–π interaction of exTTF moieties in **1·2**.[14]

The formation of the supramolecular architecture resulting from the aging of **1·2** is reversible and was successfully reversed through the addition of $CHCl_3$ to a solution of **1·2** in MCH. Throughout the experiments with a partially aged solution of **1·2** (1.25×10^{-4} M) in MCH, two trends emerged: first, a blue shift of the maxima at 391 and 461 nm, and second, an increase in intensity of the new maxima at 331, 387, and 441 nm with a simultaneous decrease in the intensity of the shoulder at 500 nm (Figure 2b). To quantify the propensity for aggregate formation, we estimated the mole fraction of aggregation (α_{agg}) at several MCH/$CHCl_3$ ratios (see the Supporting Information). The critical solvent composition, in which mixture the mole fraction of aggregation amounts to 0.5 (α_{50}), is estimated to be 60% MCH/40% $CHCl_3$. Pristine features were almost fully recovered when the concentration of $CHCl_3$ reached 80% (Figure 2b, inset). In contrast, a broad emission developed in the 550 to 700 nm range with a

maximum at 620 nm (see Figure S8 A in the Supporting Information). A complementary excitation spectrum with a maximum at 480 nm confirmed its origin (see Figure S8B in the Supporting Information). The broad and featureless π-exTTF emission was completely quenched in aged **1·2**.

Further insight into the system was gained by means of femtosecond- and nanosecond-resolved transient absorption spectroscopy. In initial experiments, we probed **1·2** in $CHCl_3$ and aged **1·2** in MCH upon excitation at 387 and 258 nm, respectively. Common to both experiments was the fast formation of a transient characterized by rather broad features (see Figure S9 in the Supporting Information) extending, in the case of aged **1·2**, all the way to 1200 nm. This species evolves from a concomitantly decaying π-exTTF excited state (see Figure S9 C in the Supporting Information). In particular, the absorption maxima, which were observed around 475 and 600 nm, were ascribed to the one-electron-reduced form of the cyanurate and the one-electron-oxidized form of the π-exTTF, respectively.[15] In other words, we observed the characteristics of an exothermically formed charge-transfer product. However, the lifetimes of **1·2** in $CHCl_3$ and aged **1·2** in MCH were quite different. Whereas the former decayed rather quickly with a lifetime of 75 ps to recover the ground state quantitatively (see Figure S9 B in the Supporting Information), we observed a slow transformation (200 ps) of the latter into a long-lived component, in which the charges tended to be delocalized, and which showed no appreciable decay on a timescale of up 3.0 ns (see Figure S9 D in the Supporting Information). Corresponding experiments involving the excitation of aged **1·2** at 532 nm for 5 ns confirmed the stability of the photoproduct; that is, we observed a transient broad absorption between 600 and 1200 nm with maxima at around 840 and 1020 nm (Figure 3 a). From a multiwavelength fitting procedure we determined a 0.3 μs lifetime for this strictly first-order process (Figure 3 b). Importantly, the presence of molecular oxygen had no impact on the lifetime of the radical-ion-pair state (see Figure S11 in the Supporting Information). This observation is critical, as it contributes to the exclusion of a triplet excited character of the photoproduct.

Information about the structural morphology of **1·2** came from X-ray diffraction (XRD), atomic force microscopy (AFM), transmission electronic microscopy (TEM), and scanning electron microscopy (SEM). First, we drop cast a freshly prepared equimolar solution of **1** and **2** (2.53×10^{-3} M) in MCH onto mica and investigated it by AFM, which indicated the collinear growth of "barrel-shaped" objects. These objects were fused together or connected by "filaments" (see Figure S12 A in the Supporting Information). All objects were uniform in height (20–35 nm) and had a planar shape (see Figure S12 B in the Supporting Information). When the same solution (2.53×10^{-3} M) was subjected to aging for a period of a week, its color changed, and a bright-orange solid began to precipitate. This precipitate was transferred onto a silicon wafer and examined by SEM (see Figure S12 C,D in the Supporting Information): unusual, homogeneous fibers were observed (Figure 4 a). These fibers were twisted, clockwise and anticlockwise, and were composed of several layers (Figure 4 b). Closer inspection

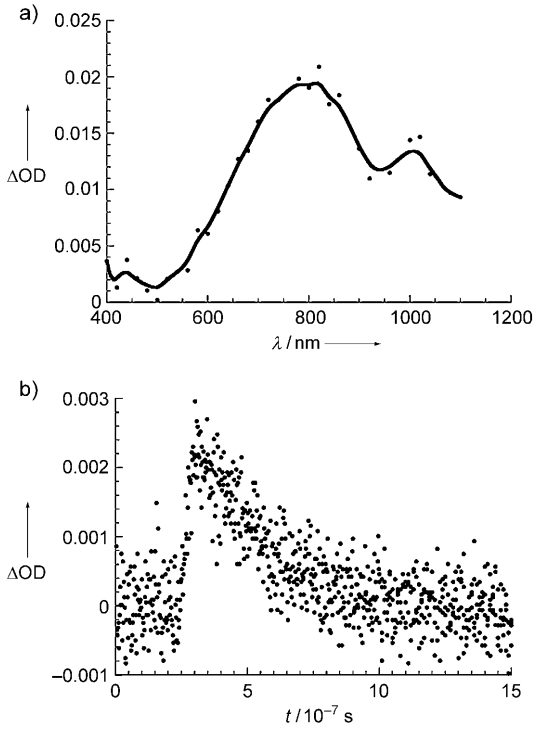

Figure 3. a) Differential absorption spectrum (visible and near-infrared) obtained upon nanosecond flash photolysis (532 nm) of **1·2** (ca. 10^{-5} M) in argon-saturated MCH with a time delay of 100 ns at room temperature. b) Time–absorption profile of the spectrum in (a) at 680 nm showing the decay of the charge-separated state in the absence of molecular oxygen.

revealed the presence of nanoribbons, which had aggregated to form fibers. The width of these nanoribbons was found to be between 35 and 50 nm. By TEM, the structure of the nanoribbons was observed as a number of stripes separated by a periodic distance of about 3.2 nm (Figure 4 c), in accordance with the experimental data obtained by XRD (see below; Figure 4 d).

Our microscopic studies suggest that the quasi-one-dimensional twisted fibers are formed by the entwining/spinning of individual nanoribbons, which are perhaps formed after the fibrillogenesis of the collinear "barrel-shaped" arrangements observed during the early-stage AFM measurements. Similar observations have been reported previously.[16]

The fiber stoichiometry (i.e., **1/2**) was established unambiguously in ^{1}H NMR spectroscopic experiments. Integration of the ^{1}H NMR spectrum of the bright-orange precipitate, that is, aged **1·2**, in [D_8]THF, gave a 4:2:2 ratio of the hydrogen atoms of the 1,3-dithiole rings of **2**, the methylene group N–CH_2 of **1**, and the imide protons of **1**, respectively. This finding is in agreement with a 1:1 stoichiometry (see Figure S13 in the Supporting Information). Furthermore, the absorption spectrum of the precipitate in MCH exactly matches that recorded after the complete aging of an equimolar mixture of **1** and **2** in MCH (see above).

XRD studies of the precipitate showed an intense and sharp small-angle reflection at 32.1 Å, which was accompanied by a number of weak reflections satisfying a reciprocal spacing ratio of 1:2:3:4 (*d* spacing): 16.2 (002), 10.8 (003), 8.1

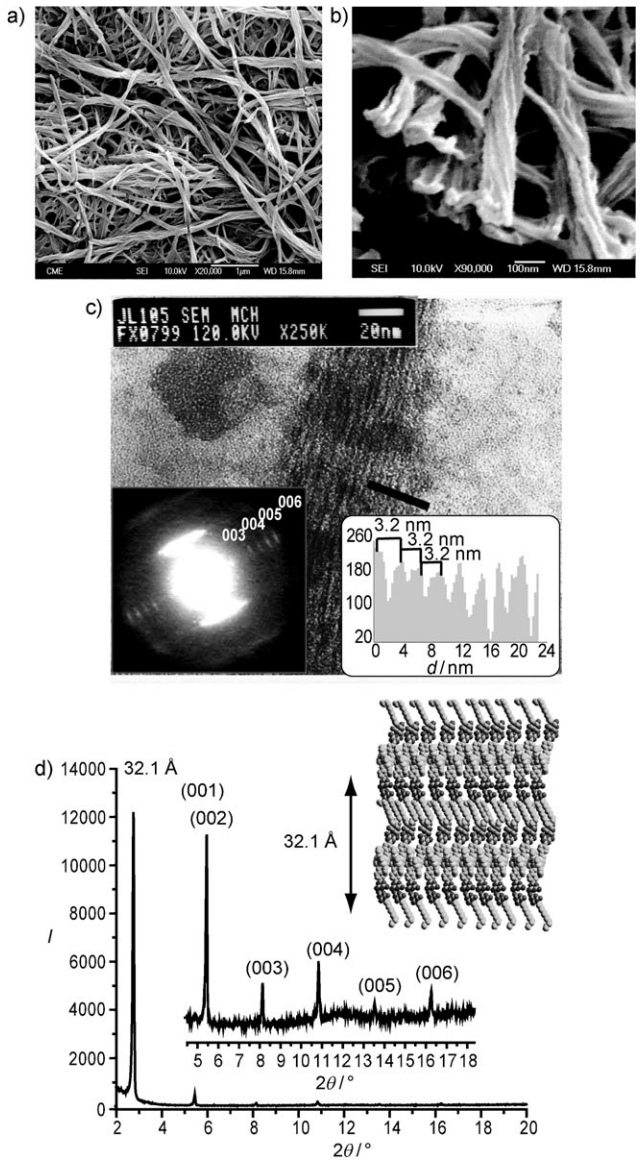

Figure 4. a) SEM image in which bunches of several fibers are perceptible (scale bar: 1 μm). b) SEM image in which bunches of twisted fibers formed by several layers are visible (scale bar: 100 nm). c) TEM image of a negative-stained isolated nanoribbon (scale bar: 20 nm), density profile of the section highlighted by the black line (inset bottom right), and electronic diffraction pattern obtained for an isolated nanoribbon by TEM at 200 kV (inset bottom left). d) XRD pattern of solvent-free films of the supramolecular nanostructure obtained after aging of an equimolar mixture of **1** and **2** in MCH (2.53×10^{-3} M).

(004) (Figure 4d). This experimental result corroborates the observation by TEM and substantiates the formation of nanoribbons with a periodic layer spacing of 32.1 Å (Figure 4d, inset). In additional test experiments with a solvent-free thin film made from a fresh equimolar mixture of **1** and **2** in MCH, no reflection peak was observed.

At this point, we must conclude that supramolecular ensembles, the formation of which is driven by hydrogen-bonding interactions, determine fiber growth. Their random character during the early stage of formation is insufficient to support an ordered and preferentially oriented growth. Therefore, during this stage, XRD and UV/Vis experiments did not show any reflection peaks or significant change in the absorption bands. Upon aging, solvophobic interactions in, for example, MCH come into play and change the situation drastically. In particular, a new pathway is now accessible that is beneficial for the quasi-one-dimensional growth. A plausible model implies the following key transformation: Hydrogen bonding of complementary **1** and **2** (the primary structure) is the starting point for the formation of extended supramolecular ensembles (the secondary structure) favored by the efficient π–π interaction between the *p*-quinoid π-exTTFs[17]; these supramolecular ensembles interdigitate laterally to form nanoribbons (the tertiary structure; see Figure S15 in the Supporting Information). Such nanoribbons are unstable and intertwine to afford fibers (the quaternary structure). The XRD patterns, TEM images, and diffraction patterns are in full agreement with this hypothesis. In fact, they corroborate that each nanoribbon is formed by several layers of the extended supramolecular architecture, and that these layers are interdigitated and separated by a periodic distance of around 3.2 nm before their aggregation into fibers. In the most likely organization of these layers, the apolar chains of **1** are placed in direct contact with the apolar solvent MCH (Figure 4d, inset). The aromatic backbone of **2**, on other hand, should be closely packed away from the apolar solvent; this arrangement would enable π–π interactions between the π-exTTFs to be fully operative (Figure 1). In effect, we believe that these interactions are decisive in causing the energetic imbalances needed to drive fiber formation.

In summary, these electroactive supramolecular ensembles at different scales represent a new type of noncovalent assembly, in which the nonplanar and redox-active π-exTTF units associate through π–π interactions, which, in turn, lead to their organization into fibers. This study has shown for the first time that butterfly-shaped π-exTTFs can facilitate the efficient organization of new 3D materials at the nanometer scale. The different nanostructures and morphologies resulting from the primary, secondary, tertiary, and quaternary architectures have been confirmed by a variety of complementary techniques (XRD, AFM, TEM, and SEM). Furthermore, photophysical measurements confirmed that the quaternary structure enables remarkable stabilization of the photogenerated radical ion pair, which has a lifetime in the millisecond range in the supramolecular assembly. In contrast, the radical ion pair of the simple complex **1·2** has a lifetime in the picosecond range.

Control over self-organizing sophisticated nanostructures based on electron-donor π-exTTFs is an important step towards their integration in photovoltaic devices.[18] In the search for photovoltaic devices with higher energy-conversion efficiencies, morphology control is a key issue.

Received: July 6, 2010
Revised: October 15, 2010
Published online: November 23, 2010

Keywords: nanoribbons · π interactions · quaternary structures · supramolecular chemistry · twisted nanofibers

[1] a) R. S. Johnson, T. Yamazaki, A. Kovalenko, H. Fenniri, *J. Am. Chem. Soc.* **2007**, *129*, 5735 – 5743; b) S. Yagai, T. Kinoshita, M. Higashi, K. Kishikawa, T. Nakanishi, T. Karatsu, A. Kitamura, *J. Am. Chem. Soc.* **2007**, *129*, 13277 – 13287; c) F. J. M. Hoeben, P. Jonkheijm, E. W. Meijer, A. P. H. J. Schenning, *Chem. Rev.* **2005**, *105*, 1491 – 1546; d) S. Yagai, T. Nakajima, T. Karatsu, K.-i. Saitow, A. Kitamura, *J. Am. Chem. Soc.* **2004**, *126*, 11500 – 11508; e) V. Balzani, *Electron Transfer in Chemistry, Vol. I–V*, Wiley-VCH, Weinheim, **2001**.

[2] a) F. J. M. Hoeben, M. Wolffs, J. Zhang, S. De Feyter, P. Leclère, A. P. H. J. Schenning, E. W. Meijer, *J. Am. Chem. Soc.* **2007**, *129*, 9819 – 9828; b) V. Huber, M. Katterle, M. Lysetska, F. Würthner, *Angew. Chem.* **2005**, *117*, 3208 – 3212; *Angew. Chem. Int. Ed.* **2005**, *44*, 3147 – 3151; c) T. S. Balaban, *Acc. Chem. Res.* **2005**, *38*, 612 – 623; d) T. S. Balaban, A. D. Bhise, M. Fischer, M. Linke-Schaetzel, C. Roussel, N. Vanthuyne, *Angew. Chem.* **2003**, *115*, 2190 – 2194; *Angew. Chem. Int. Ed.* **2003**, *42*, 2140 – 2144.

[3] a) M. M. Elmahdy, X. Dou, M. Mondeshki, G. Floudas, H.-J. Butt, H. W. Spiess, K. Müllen, *J. Am. Chem. Soc.* **2008**, *130*, 5311 – 5319; b) T. Yamamoto, T. Fukushima, A. Kosaka, W. Jin, Y. Yamamoto, N. Ishii, T. Aida, *Angew. Chem.* **2008**, *120*, 1696 – 1699; *Angew. Chem. Int. Ed.* **2008**, *47*, 1672 – 1675; c) Y. Yamamoto, T. Fukushima, Y. Suna, N. Ishii, A. Saeki, S. Seki, S. Tagawa, M. Taniguchi, T. Kawai, T. Aida, *Science* **2006**, *314*, 1761 – 1764.

[4] a) Ž. Tomović, J. van Dongen, S. J. George, H. Xu, W. Pisula, P. Leclère, M. M. J. Smulders, S. De Feyter, E. W. Meijer, A. P. H. J. Schenning, *J. Am. Chem. Soc.* **2007**, *129*, 16190 – 16196; b) S. J. George, Ž. Tomović, M. M. J. Smulders, T. F. A. de Greef, P. E. L. G. Leclère, E. W. Meijer, A. P. H. J. Schenning, *Angew. Chem.* **2007**, *119*, 8354 – 8359; *Angew. Chem. Int. Ed.* **2007**, *46*, 8206 – 8211; c) A. Ajayaghosh, V. K. Praveen, *Acc. Chem. Res.* **2007**, *40*, 644 – 656.

[5] a) J. Puigmartí-Luis, V. Laukhin, Á. Pérez del Pino, J. Vidal-Gancedo, C. Rovira, E. Laukhina, D. B. Amabilino, *Angew. Chem.* **2007**, *119*, 242 – 245; *Angew. Chem. Int. Ed.* **2007**, *46*, 238 – 241; b) J. L. López, E. M. Pérez, P. M. Viruela, R. Viruela, E. Ortí, N. Martín, *Org. Lett.* **2009**, *11*, 4524 – 4527; c) for a recent review, see: M. Hasegawa, M. Iyoda, *Chem. Soc. Rev.* **2010**, *39*, 2420 – 2427.

[6] a) F. Würthner, C. Bauer, V. Stepanenko, S. Yagai, *Adv. Mater.* **2008**, *20*, 1695 – 1698; b) X. Zhang, Z. Chen, F. Würthner, *J. Am. Chem. Soc.* **2007**, *129*, 4886 – 4887; c) T. E. Kaiser, H. Wang, V. Stepanenko, F. Würthner, *Angew. Chem.* **2007**, *119*, 5637 – 5640; *Angew. Chem. Int. Ed.* **2007**, *46*, 5541 – 5544.

[7] a) J. Wang, Y. Shen, S. Kessel, P. Fernandes, K. Yoshida, S. Yagai, D. G. Kurth, H. Möhwald, T. Nakanishi, *Angew. Chem.* **2009**, *121*, 2200 – 2204; *Angew. Chem. Int. Ed.* **2009**, *48*, 2166 – 2170; b) C. Reiriz, R. J. Brea, R. Arranz, J. L. Carrascosa, A. Garibotti, B, Manning, J. M. Valpuesta, R. Eritja, L. Castedo and J. R. Granja, *J. Am. Chem. Soc.* **2009**, *131*, 11335 – 11337; c) R. J. Brea, L. Castedo, J. R. Granja, L. Sánchez, M. Á. Herranz, N. Martín, W. Seitz, D. M. Guldi, *Proc. Natl. Acad. Sci. USA* **2007**, *104*, 5291 – 5294.

[8] a) S. Xiao, M. Myers, Q. Miao, S. Sanaur, K. Pang, M. L. Steigerwald, C. Nuckolls, *Angew. Chem.* **2005**, *117*, 7556 – 7560; *Angew. Chem. Int. Ed.* **2005**, *44*, 7390 – 7394; b) Q. Chen, T. Chen, G.-B. Pan, H.-J. Yan, W.-G. Song, L.-J. Wan, Z.-T. Li, Z.-H. Wang, B. Shang, L.-F. Yuan, J.-L. Yang, *Proc. Natl. Acad. Sci. USA* **2008**, *105*, 16849 – 16854; c) D. Miyajima, K. Tashiro, F. Araoka, H. Takezoe, J. Kim, K. Kato, M. Takasata, T. Aida, *J. Am. Chem. Soc.* **2009**, *131*, 44 – 45.

[9] a) E. M. Pérez, L. Sánchez, G. Fernández, N. Martín, *J. Am. Chem. Soc.* **2006**, *128*, 7172 – 7173; b) G. Fernández, E. M. Pérez, L. Sánchez, N. Martín, *J. Am. Chem. Soc.* **2008**, *130*, 2410 – 2411; c) G. Fernández, E. M. Pérez, L. Sánchez, N. Martín, *Angew. Chem.* **2008**, *120*, 1110 – 1113; *Angew. Chem. Int. Ed.* **2008**, *47*, 1094 – 1097; d) G. Fernández, L. Sánchez, E. M. Pérez, N. Martín, *J. Am. Chem. Soc.* **2008**, *130*, 10674 – 10683; e) E. M. Pérez, N. Martín, *Chem. Soc. Rev.* **2008**, *37*, 1512 – 1519; f) A. Molina-Ontoria, G. Fernández, M. Wielopolski, C. Atienza, L. Sánchez, A. Gouloumis, T. Clark, N. Martín, D. M. Guldi, *J. Am. Chem. Soc.* **2009**, *131*, 12218 – 12229.

[10] S. Yagai, M. Higashi, T. Karatsu, A. Kitamura, *Chem. Mater.* **2004**, *16*, 3582 – 3585.

[11] A. G. Bielejewska, C. A. Marjo, L. J. Prins, P. Timmerman, F. de Jong, D. N. J. Reinhoudt, *J. Am. Chem. Soc.* **2001**, *123*, 7518 – 7533.

[12] F. J. M. Hoeben, M. J. Pouderoijen, A. P. H. J. Schenning, E. W. Meijer, *Org. Biomol. Chem.* **2006**, *4*, 4460 – 4462.

[13] To determine the size of the supramolecular assemblies formed in dilute solutions, we carried out dynamic light scattering (DLS) measurements on complex **1·2** in $CHCl_3$ ($0.013\ g\,L^{-1}$). The measurements showed the presence of a broad unimodal distribution centered at an average hydrodynamic radius of RH = 49 nm, a value which was reproducible at different angles (see Figure S3 in the Supporting Information). This observation confirms the formation of large aggregates in solution by means of hydrogen-bond interactions as the driving force.

[14] To compare the electronic spectrum of compound **2** with that of its analogue, **3**, without the exTTF moiety, we synthesized compound **3** (J. Henkin, D. J. Davidson, G. S. Sheppard, K. W. Woods, R. W. McCroskey, *PCT Int. Appl.* **1999**, 66) and studied the features of its electronic spectrum. The UV/Vis spectra recorded in both $CHCl_3$ and MCH showed a broad absorption band in the visible region ($\lambda_{max} = 323$ nm). As expected, this band was not shifted after aging for over a week. We could thus rule out a π–π interaction between triazine and stilbene moieties as the driving force for supramolecular assembly.

[15] The solution electrochemistry of **1**, **2**, and a 1:1 mixture of **1·2** was investigated by cyclic voltammetry in $CHCl_3$. Ag/Ag^+ was used as the reference electrode. Pt wire was the counter electrode, and glassy carbon (GC) was used as the working electrode. Although the experimental data showed that the cyanurate moiety is a better acceptor than the *s*-triazine unit, the formation of the radical anion of the *s*-triazine unit cannot be ruled out (see Figure S10 in the Supporting Information).

[16] G. Das, L. Ouali, M. Adrian, B. Baumeister, K. J. Wilkinson, S. Matile, *Angew. Chem.* **2001**, *113*, 4657 – 4661; *Angew. Chem. Int. Ed.* **2001**, *40*, 4793 – 4797.

[17] Preliminary density functional theory (DFT) calculations performed at the BH&H/6-31G** level showed that the *p*-quinoid π-exTTF units give rise to very effective π–π interactions. The lateral benzene rings form π–π dimers with interplanar distances of 3.71 and 3.39 Å and binding energies of −8.56 and −8.20 kcal mol^{-1} (Figure S14a,b, respectively). The combination of these interactions enables stacking of the *p*-quinoid π-exTTF units as sketched for the hexamer depicted in Figure S14c, for which a binding energy of −68.18 kcal mol^{-1} was calculated. On the other hand, STM studies of π-exTTF on a gold surface revealed that *p*-quinoid π-exTTF molecules are able to form up to three stacked layers: R. Otero, D. Écija, G. Fernández, J. M. Gallego, L. Sánchez, N. Martín, R. Miranda, *Nano Lett.* **2007**, *7*, 2602 – 2607. AFM, ^1H NMR spectroscopy, and DLS have also shown the strong aggregation of π-exTTF-containing dendrimers in solid, liquid, and gas phases (see Ref. [9d]).

[18] N. Martín, L. Sánchez, M. A. Herranz, B. Illescas, D. M. Guldi, *Acc. Chem. Res.* **2007**, *40*, 1015 – 1024.

